

# Miniaturized 3-Bit Frequency-Reconfigurable Monopole Antenna with a Meander-Line

Xueyang Hu<sup>1</sup>, Yun Liu<sup>1</sup>, and Yueyou Yang<sup>1</sup>

<sup>1</sup>Nanjing University of Aeronautics and Astronautics

April 4, 2023

## Abstract

A novel 3-bit frequency-reconfigurable antenna (FRA) with miniaturized dimensions is realized with a meander line. The frequency reconfiguration of the antenna is achieved by introducing  $N$  RF p-i-n diodes into the meander line. The related parts of the meander line with different lengths are bypassed or included into the antenna by switching on or off the diodes, resulting in  $2N$  switchable size lengths of the antenna and equally spaced operating frequencies. A 3-bit meander-line reconfigurable antenna ( $N=3$ ) is designed, and the simulated and measured results agree well. The antenna provides  $2^3=8$  independent switchable states, with the operating frequencies covering a wide switchable frequency range from 1.04 GHz to 1.51 GHz and the working bandwidths varying from 80 MHz to 150 MHz. The number of working states is optimally large, considering the number of switches used. Besides, this work has an acceptable peak gain of 1.59 dBi regarding the miniaturized total dimension of  $0.17 \lambda \times 0.07 \lambda$  ( $\lambda$  is the wavelength of the lowest working frequency), which is more compact than many published FRAs.

## Miniaturized 3-Bit Frequency-Reconfigurable Monopole Antenna with a Meander-Line

Xueyang Hu, Yun Liu\* and Yueyou Yang

*Nanjing University of Aeronautics and Astronautics, Nanjing 211106, China*

lycloud1978@163.com\*

Abstract—A novel 3-bit frequency-reconfigurable antenna (FRA) with miniaturized dimensions is realized with a meander line. The frequency reconfiguration of the antenna is achieved by introducing  $N$  RF p-i-n diodes into the meander line. The related parts of the meander line with different lengths are bypassed or included into the antenna by switching on or off the diodes, resulting in  $2^N$  switchable size lengths of the antenna and equally spaced operating frequencies. A 3-bit meander-line reconfigurable antenna ( $N=3$ ) is designed, and the simulated and measured results agree well. The antenna provides  $2^3=8$  independent switchable states, with the operating frequencies covering a wide switchable frequency range from 1.04 GHz to 1.51 GHz and the working bandwidths varying from 80 MHz to 150 MHz. The number of working states is optimally large, considering the number of switches used. Besides, this work has an acceptable peak gain of 1.59 dBi regarding the miniaturized total dimension of  $0.17 \lambda \times 0.07 \lambda$  ( $\lambda$  is the wavelength of the lowest working frequency), which is more compact than many published FRAs.

*Introduction:* With the rapid development of modern wireless communication systems, RF front-ends are required to operate at multiple frequency bands, and the number of integrated antenna and total dimensions is highly increased. To solve the problems, reconfigurable antennas have been extensively studied recently.

Reconfigurable antennas can be classified into three types, namely, frequency-reconfigurable antennas (FRAs) [1]-[10], polarization-reconfigurable antennas [11], and radiation pattern reconfigurable antennas [12]. Among them, FRAs have attracted substantial attention and been intensively studied. The frequency of an FRA can be continuously tuned using varactors [1]-[5] or discretely switched using RF-switches [6]-[10]. Frequency

reconfigurability has been achieved on various types of antennas, such as microstrip patch antennas (MSAs) [1], [2], [9], dipole antennas [3], patch-slot antennas (PSAs) [6], microstrip monopole antennas (MMAs) [7], microstrip slot antenna (MSA) [8], and planar inverted-F antennas (PIFAs) [10]. Majority of FRAs tune/switch the resonant frequencies by reconfiguring the current flow path on the antenna or reshaping the antenna structure, changing the equivalent electrical lengths of antennas in addition.

Nonetheless, many of these published FRAs fail to take miniaturization into account, which is critical especially when FRAs are used in handheld devices. Typically, antenna miniaturization is accomplished by folding the radiation branch of the antenna [13], [14], by selecting an antenna patch loaded with a specialized shape [15] or a shorting wall [16], and by introducing metasurfaces [17] or metamaterial structures [18]. The most common method of antenna miniaturization is to use a meander line. In [14], a miniaturized monopole chip antenna with meander lines on the first and third layers is presented, greatly reducing the antenna's size at lower and upper bands.

Furthermore, many published FRAs load too many switches while only providing a limited number of operational states. Fortunately, binary reconfiguration can successfully resolve this problem by realizing  $2^N$  switchable states with  $N$  switches. A 3-bit binary reconfigurable PIFA with eight independent states covering a working frequency range from 1.52 GHz to 2.25 GHz is developed by using three MEMS switches in [10]. The presented FRA is miniaturized by the meander line in [7], and only three states are achieved using two diodes.

In this study, a miniature 3-bit frequency-reconfiguring monopole antenna with a meander-line is proposed. It employs three switches to achieve  $2^3$  states, which is the maximum number of states. The structure can be extended for achieving binary FRA with larger number of bits.

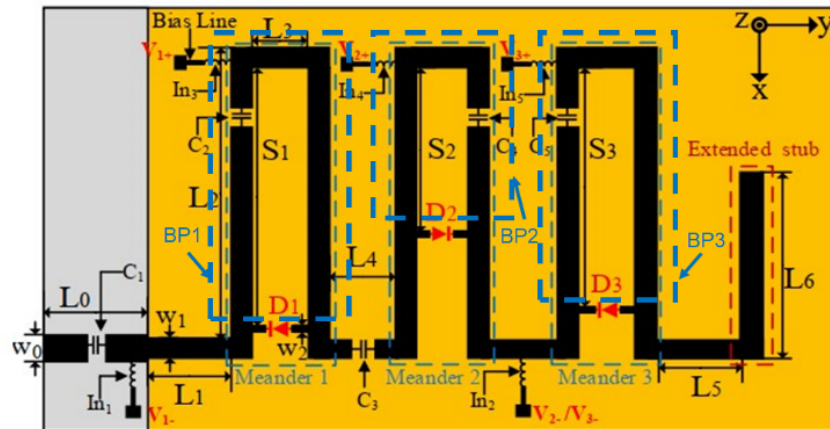
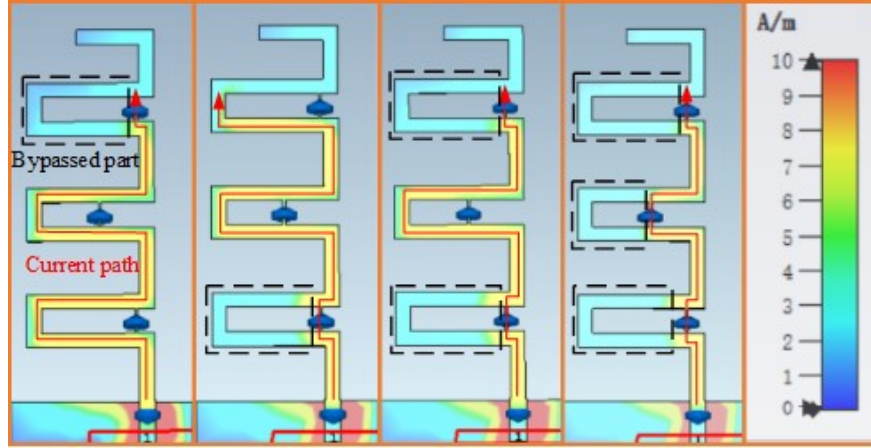


**Fig. 1** Geometry of the proposed antenna.  $L_0 = 5$  mm,  $L_1 = 6$  mm,  $L_2 = 12.4$  mm,  $L_3 = 2.8$  mm,  $L_4 = 6$  mm,  $L_5 = 4.4$  mm,  $L_6 = 8.6$  mm,  $W_0 = 1.8$  mm,  $W_1 = 1.6$  mm,  $W_2 = 0.3$  mm,  $S_1 = 10.3$  mm,  $S_2 = 6.2$  mm,  $S_3 = 9.8$  mm.



(a) (b) (c) (d)

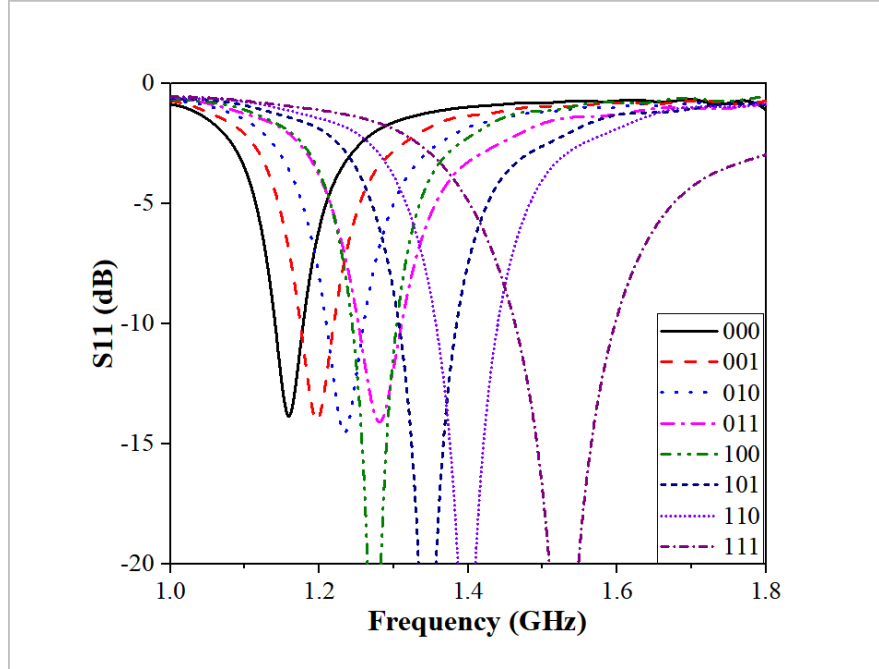
**Fig. 2.** Surface current distributions for state 001 (a), state 100 (b), state 101 (c), and state 111 (d).

*Antenna Configuration and Miniaturization Design:*

Fig. 1 shows a miniaturized binary frequency-reconfigurable meander-line antenna. The main transmission line of the antenna is folded three times at different locations. Three meanders have uniform width.

As shown in Fig. 1, three PIN diode switches are introduced at the meander of the main transmission line, and short narrow strips extended from the meanders are used to place PIN diodes. By switching on the PIN diode switch, the relevant parts of the bending structure with different lengths are bypassed from the antenna structure. The current flows directly from the PIN switch without passing through the bypassed transmission line section, resulting in a shorter actual path length of the current. Consequently, the operating frequency of the antenna increases. On the contrary, the corresponding parts are connected to the antenna structure by turning off the switch. For example, when the PIN diode  $D_1$  is turned on, the BP1 section is bypassed, and the current passes directly through the switch  $D_1$  without going through BP1. As a result, the actual path length of the current is shortened, and the frequency of the antenna is correspondingly increased. Different settings of the on/off status of  $D_1$ ,  $D_2$ , and  $D_3$  result in changes in the effective length of the antenna, which can achieve  $2^3$  different operating frequencies and realize frequency reconfigurability.

As for the biasing circuit,  $C_1$ ,  $C_2$ ,  $C_3$ ,  $C_4$ , and  $C_5$  achieve DC-blocking, dividing the antenna into multiple transmission line segments with different DC voltages.  $In_1$  and  $In_2$ , as RC chokes, are connected to ground via holes and achieve DC grounding as one end of the PIN diodes  $D_1$ ,  $D_2$ , and  $D_3$ . The three control voltages,  $V_1$ ,  $V_2$ , and  $V_3$  are respectively connected to the other end of  $D_1$ ,  $D_2$ , and  $D_3$  via inductors  $In_3$ ,  $In_4$ , and  $In_5$ .



*3-Bit Frequency-Reconfiguration Design:* The influence of the bypassed part on the electrical length of the antenna is assumed to be negligible, and the current is uniformly distributed in the bending line. Switches  $D_1$ ,  $D_2$ , and  $D_3$  are assigned to the centers of meanders 1, 2, and 3, with different positions in the x-axis direction. To achieve binary frequency reconfiguration, the length of the bypassed transmission line  $S_1$ ,  $S_2$ , and  $S_3$  are proposed to satisfy:  $S_1 > S_2 > S_3$ . By operating the three switches as shown in Table I, eight independent antenna working states can be obtained, with "1" representing "on" and "0" representing "off" (i.e., achieving the 3-bit frequency reconfiguration).

Fig. 2 depicts the simulated surface current distribution at various resonant frequencies. When one of the switches is turned on, a portion of the corresponding meander is bypassed, resulting in a new structure that can be equivalent to an open stub, as shown in the figure. As a result, the current path on the meander line is reconfigured, as indicated by the red curves, avoiding the bypassed part and flowing directly through the p-i-n diode. Therefore, the equivalent electrical length of the meander is reduced. When the switch is turned off, the related part of the meander is incorporated into the meander line, increasing the antenna's electric length.

In Fig. 2(a), the current density of the bypassed part of meander three is significantly reduced by turning on  $D_3$ , reducing the corresponding electrical length of the antenna. In addition, the resonant frequency shifts to a higher band compared with the condition when  $D_3$  is turned off.

When either of the switches, as shown in Figs. 2(b) and 2(c), are turned on, the longer the shortened current path, the shorter the equivalent electrical length of the meander line, and the higher the working frequency of the antenna are obtained.

Finally, in Fig. 2(d), the highest working frequency is attained at state 111 because the shortest current path on the meander line and the smallest equivalent electrical length of the antenna, which resulted from all three switches being turned on.

The electrical length obviously decreases sequentially from state 000 to state 111, resulting in a gradual increase in the resonant frequency of the antenna. Therefore, the frequency range of the roughly reconfigurable can be first determined based on  $f_H$  and  $f_L$ , followed by the resonance frequencies of the eight different

operating states. Owing to miniaturization, the range of reconfigurable frequencies is limited by the size of the antenna. Thus, the operating frequency bands of each state must be optimized to ensure that they are clear and evenly distributed within a finite frequency range and minimize overlap as much as possible. All the simulation and parameter optimization of the antenna proposed in this study are realized by computer simulation technology (CST) software.

The antenna proposed in this study is designed to operate in the frequency range of 1.04–1.51 GHz with a bandwidth from 80 MHz to 150 MHz. In the practical design of the reconfigurable antenna, the intermediate dielectric layer employs Rogers RO4003C substrate, with a relative dielectric constant of 3.38 and a thickness of 0.813 mm. In addition, the RF PIN diodes from Skyworks with a PIN of SMP1331-079LF are used [19], and the diode is equivalent to a resistance of  $1.7 \Omega$  and a capacitance of 0.18 pF at the on and off states in simulation, respectively.

The optimized parameters obtained from the simulation are:  $L_0 = 5$  mm,  $L_1 = 6$  mm,  $L_2 = 12.4$  mm,  $L_3 = 2.8$  mm,  $L_4 = 6$  mm,  $L_5 = 4.4$  mm,  $L_6 = 8.6$  mm,  $W_0 = 1.8$  mm,  $W_1 = 1.6$  mm,  $W_2 = 0.3$  mm,  $S_1 = 10.3$  mm,  $S_2 = 6.2$  mm, and  $S_3 = 9.8$  mm. The values of the bias inductors  $In_1, In_2, In_3, In_4,$  and  $In_5$  are 180 nH. The values of the DC blocking capacitors  $C_1, C_2, C_3, C_4,$  and  $C_5$  are 100 pF.

**Table I:** Conditions of diodes in different states.

States								
Diodes	000	001	010	011	100	101	110	111
$D_1$	Off	Off	Off	Off	On	On	On	On
$D_2$	Off	Off	On	On	Off	Off	On	On
$D_3$	Off	On	Off	On	Off	On	Off	On

The results show that  $S_3$  is larger than  $S_2$  after optimization. This is because the initial assumption is that the current distribution along the

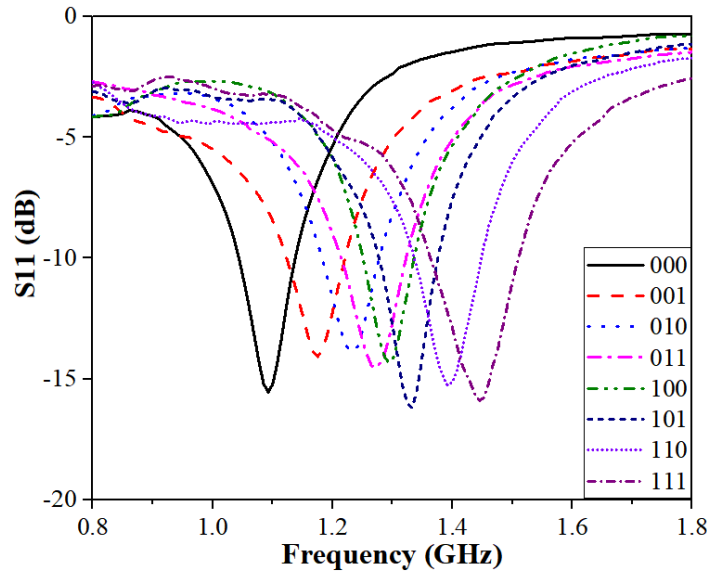


**Fig. 3.** Simulated reflection coefficient at different states of the proposed 3-bit FRA.

**Fig. 4** Measured reflection coefficient at different states and photograph of the proposed 3-bit FRA.

meander line is uniform, but the contribution of each bypassed section on frequency reconfiguration is not proportional to the length. As a result, the current distribution along the meander line is varying, and  $S_3$  becomes larger than  $S_2$ . Aside from the phenomenon of increasing  $S_3$ , Fig. 2 shows that the current path of each state is fundamentally the same as the equivalent structure of the corresponding state, and the bypassed sections are with no current.

Fig. 3 depicts the ultimate simulated  $S_{11}$  results at various states of the proposed antenna. The eight states are completely self-contained and have good impedance-matching performance over a frequency range of 1.14–1.6 GHz. Within the operating frequency band, the return loss,  $S_{11}$ , is less than 10 dB. At the lowest working frequency (1.14 GHz), the size of the antenna is reduced to  $0.19 \lambda_0 \times 0.08 \lambda_0$ .

**Table II.** Simulated and measured resonance frequencies and operating bandwidths.

State	Sim. freq	Mea.freq	Sim.BW	Mea.BW
000	1.16GHz	1.09GHz	40MHz	90MHz
001	1.20GHz	1.17GHz	50MHz	100MHz
010	1.23GHz	1.23GHz	60MHz	90MHz
011	1.28GHz	1.27GHz	60MHz	110MHz
100	1.27GHz	1.29GHz	65MHz	80MHz
101	1.35GHz	1.33GHz	80MHz	100MHz
110	1.40GHz	1.39GHz	90MHz	110MHz
111	1.53GHz	1.44GHz	140MHz	150MHz

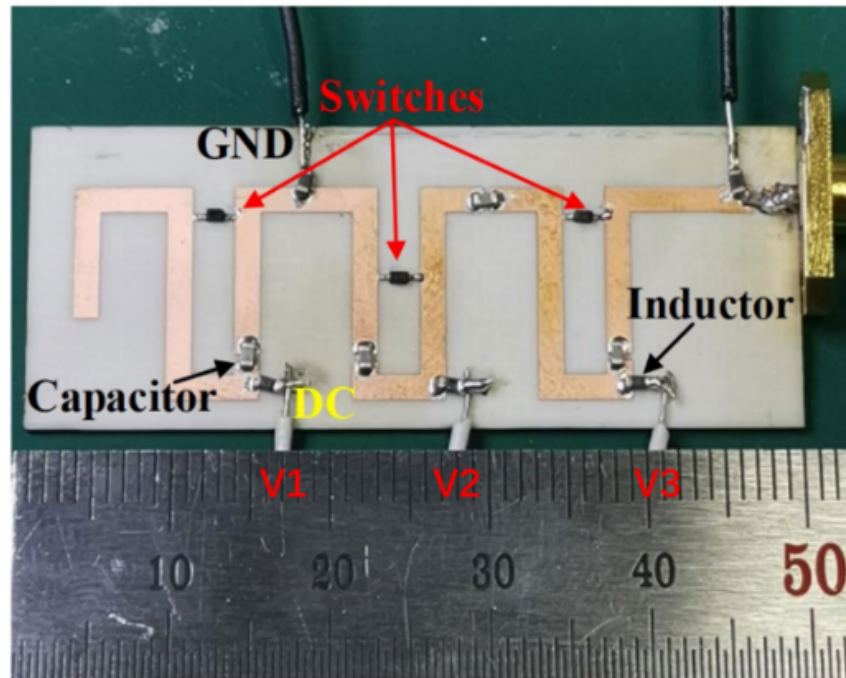


**Fig. 5.** Photograph of the proposed 3-bit FRA.

*Results and discussion:* The measured results of the reflection coefficient and the photograph of the antenna prototype are given in Fig. 4 and Fig. 5. The S<sub>11</sub> results are measured with an Agilent N5230A vector network analyzer. Eight independent states are observed with the operating frequency switched from 1.04 GHz to 1.51 GHz. Good impedance matching and low return loss are obtained for each state, and the simulated and measured working frequency and bandwidth at each state are compared in Table II. Except for a small frequency shift of approximately 74 MHz on average for each state, agreement between the simulation and the measurement results is good. The measured bandwidths are larger than the simulated ones, and this is possibly caused by the resistive loading of the biasing components and switches in practical designs. Furthermore, Fig. 4(a) shows a few unexpected perturbations on the S<sub>11</sub> curves caused by the parasitic effect of biasing lumped elements. Fig. 5 gives a photograph of the fabricated prototype antenna.

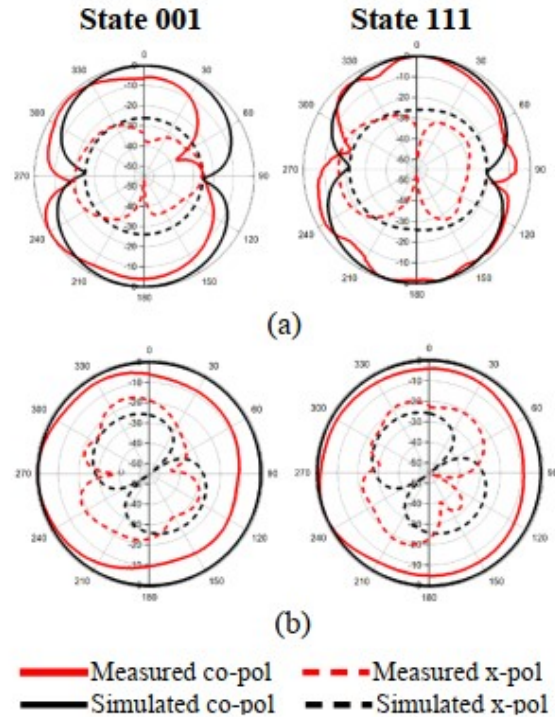


**Fig. 6.** Simulated (dashed line) and measured (solid line) radiation patterns at resonant frequencies of state 001 and state 111. (a) E-plane; (b) H-plane.

TABLE III. Comparison of several frequency reconfigurable antennas

Ref	Type	Size	Freq (GHz)	No. PIN	No. states	Binary reconfigurable	Peak gain
[1]	MPA	0.44×0.44	1.64-2.12	8	5	No	<b>6.0</b>
[6]	MPSA	0.13×0.21	1.98-3.59	5	9	No	<b>4.8</b>
[7]	MMA	0.04×0.01	0.72-2.4	2	3	Yes	<b>7.6</b>
[8]	MSA	0.52×0.48	2.2-4.75	5	6	No	<b>4.1</b>
This work	MMA	0.17×0.07	1.04-1.51	3	8	Yes	<b>1.59</b>

In the comparison in Table III, the antenna proposed in this study uses three switches to achieve 2<sup>3</sup> states,

which is the maximum number of reconfigurable states. Compared with previous FRAs, this antenna has a smaller size and achieves more states using fewer switches.

In far-field situation, the proposed antenna aims to maintain bidirectional radiation characteristics in the E-plane (yz-plane) and nearly omnidirectional pattern in the H-plane (xz-plane) for all the eight states, which is in accordance with the far-field patterns of typical printed MMA. This work is tested in an anechoic chamber. Fig. 6 shows the simulated and measured far-field results at state 111, where radiation patterns are most possibly changed because of the dc supplies for the three switches. The simulated far-field results still agree well with the measured output. The simulated gain for all states varies from 1.11 dBi to 1.59 dBi, where the peak gain is obtained at state 000 because all switches are turned off, and the radiation efficiency is larger than 84%. However, the measured peak gain is 0.5 dBi because the p-i-n diodes and many lumped elements introduce some losses.

*Conclusion:* A 3-bit frequency reconfigurable meander-line MMA is proposed. The antenna has  $2^3 = 8$  independent narrow band states. The number of states is optimally large in terms of the number of switches used because of the antenna's binary reconfigurability. The measured results agree well with the simulated ones, and good impedance matching characteristics and acceptable bandwidth are achieved on each state, covering a considerable frequency range from 1.01 GHz to 1.54 GHz. This antenna has similar far-field radiation characteristics as the traditional MMA and features in immensely miniaturized size.

*Acknowledgement:*

This work was supported by National Natural Science Foundation of China under grant 62071228.

## References

- 1 G. Lei, and L. Kwai-Man, "Frequency-Reconfigurable Low-Profile Circular Monopolar Patch Antenna," *IEEE Trans. Antennas Propag.*, vol. 62, no. 7, pp. 3443-3449, 2014.
- 2 L. Ge, M. Li, J. Wang, and H. Gu, "Unidirectional Dual-Band Stacked Patch Antenna With Independent Frequency Reconfiguration," *IEEE Antennas Wireless Propag. Lett.*, vol. 16, pp. 113-116, 2017.
- 3 J.-B. Ko, and D. Kim, "A Wideband Frequency-Tunable Dipole Antenna Based on Antiresonance Characteristics," *IEEE Antennas Wireless Propag. Lett.*, vol. 16, pp. 3067-3070, 2017.
- 4 S.-C. Tang, X.-Y. Wang and J.-X. Chen, "Low-Profile Frequency-Reconfigurable Dielectric Patch Antenna and Array Based on New Varactor-Loading Scheme," in *IEEE Transactions on Antennas and Propagation*, vol. 69, no. 9, pp. 5469-5478, Sept. 2021, doi: 10.1109/TAP.2021.3060053.
- 5 M. Wang et al., "Miniaturization of Frequency-Reconfigurable Antenna Using Periodic Slow-Wave Structure," in *IEEE Transactions on Antennas and Propagation*, vol. 69, no. 11, pp. 7889-7894, Nov. 2021, doi: 10.1109/TAP.2021.3076570.
- 6 H. A. Majid, M. K. Abdul Rahim, M. R. Hamid, N. A. Murad, and M. F. Ismail, "Frequency-Reconfigurable Microstrip Patch-Slot Antenna," *IEEE Antennas Wireless Propag. Lett.*, vol. 12, pp. 218-220, 2013.
- 7 Y. Tawk, A. El-Amine, S. Saab, J. Costantine, F. Ayoub, and C. G. Christodoulou, "A Software-Defined Frequency-Reconfigurable Meandered Printed Monopole," *IEEE Antennas Wireless Propag. Lett.*, vol. 17, no. 2, pp. 327-330, 2018.
- 8 H. A. Majid, M. K. A. Rahim, M. R. Hamid, and M. F. Ismail, "A Compact Frequency-Reconfigurable Narrowband Microstrip Slot Antenna," *IEEE Antennas Wireless Propag. Lett.*, vol. 11, pp. 616-619, 2012.
- 9 A. Boukarkar, X. Q. Lin, Y. Jiang, and X. F. Yang, "A Compact Frequency-Reconfigurable 36-States Patch Antenna for Wireless Applications," *IEEE Antennas Wireless Propag. Lett.*, vol. 17, no. 7, pp. 1349-1353, 2018.
- 10 G. Chaabane, V. Madrangeas, M. Chatras, E. Arnaud, L. Huitema, and P. Blondy, "High-linearity 3-bit frequency-tunable planar inverted-F antenna for RF applications," *IEEE Antennas Wireless Propag. Lett.*,

vol. 16, pp. 983–986, 2017.

11 J. Zhou and F. Xu, "A Low Profile Polarization Reconfigurable Antenna Based on Substrate Integrated Waveguide," 2022 International Conference on Microwave and Millimeter Wave Technology (ICMMT), Harbin, China, 2022, pp. 01-03, doi: 10.1109/ICMMT55580.2022.10022690.

12 J. Lu, H. C. Zhang, P. H. He, M. Wang and T. J. Cui, "Pattern Reconfigurable Yagi Antenna Based on Active Corrugated Stripline," in IEEE Transactions on Antennas and Propagation, vol. 71, no. 1, pp. 1011-1016, Jan. 2023, doi: 10.1109/TAP.2022.3215813.

13 D. E. Brocker, Z. H. Jiang, M. D. Gregory, and D. H. Werner, "Miniaturized Dual-Band Folded Patch Antenna with Independent Band Control Utilizing an Interdigitated Slot Loading," IEEE Trans. Antennas Propag., vol. 65, no. 1, pp. 380-384, 2017.

14 Z.-X. Xia, K. W. Leung, M. W. K. Lee, and N. Yang, "Miniature Dual-Band Meander-Line Monopole Chip Antenna with Independent Band Control," IEEE Antennas Wireless Propag. Lett., vol. 18, no. 9, pp. 1873-1877, 2019.

15 Z. Wang, Y. Yin, J. Wu, and R. Lian, "A Miniaturized CPW-Fed Antipodal Vivaldi Antenna with Enhanced Radiation Performance for Wideband Applications," IEEE Antennas Wireless Propag. Lett., vol. 15, pp. 16-19, 2016.

16 A. Boukarkar, X. Q. Lin, Y. Jiang, and Y. Q. Yu, "Miniaturized Single-Feed Multiband Patch Antennas," IEEE Trans. Antennas Propag., vol. 65, no. 2, pp. 850-854, 2017.

17 W. E. I. Liu, Z. N. Chen, X. Qing, J. Shi, and F. H. Lin, "Miniaturized Wideband Metasurface Antennas," IEEE Trans. Antennas Propag., vol. 65, no. 12, pp. 7345-7349, 2017.

18 K. Sun, S. Han, J. H. Choi, and J. K. Lee, "Miniaturized Active Metamaterial Resonant Antenna With Improved Radiation Performance Based on Negative-Resistance-Enhanced CRLH Transmission Lines," IEEE Antennas Wireless Propag. Lett., vol. 17, no. 7, pp. 1162-1165, 2018.

19 Skyworks Solutions Inc, Skyworks Data Sheet. [Online]. Available: <http://www.skyworksinc.com/>